Coupled thermo-mechanical model based comparison of friction stir welding processes of AA2024-T3 in different thicknesses

Z. Zhang · J. T. Chen · Z. W. Zhang · H. W. Zhang

Abstract A fully coupled thermo-mechanical finite element model was used to study the friction stir welding process of AA2024-T3 in different thicknesses. The computational results show that the material flows on the retreating and the front sides are higher. So, the slipping rates on the retreating and the front sides are lower than the ones on the trailing and advancing sides. This is the reason that the heat fluxes on the trailing and the advancing sides are higher, which leads to the fact that the temperatures are higher in this region for both thin and thick plates. The energy entering the welding plate accounts for over 50% in the total energy and about 85% in the energy comes from the frictional heat in FSW of AA2024-T3 and the balance from the mechanical effects. The stirring effect of the welding tool becomes weaker in FSW of thick plates. With consideration of the material deformations and the energy conversions, FSW of thin plates shows advantages.

Introduction

Friction stir welding (FSW) is a solid state joining technique. Since its invention, FSW has been used for joining aluminum alloys, magnesium alloys, titanium alloys, copper alloys, stainless steels, and even metal matrix composites [1–8]. In FSW, the maximum temperature is lower than the melting point T_m of the base metal but is higher than the recrystallization temperature 0.4 T_m (K). Temperatures and material behaviors are the main factors to affect the grain sizes [9] and the precipitations [10, 11]. Friction and plastic deformation are the two reasons to the temperature rises in FSW. The ratio of plastic dissipation/frictional dissipation is about 30% for FSW of AA6061-T6 [12]. So, friction is much more important for the heat generations in the FSW processes. The increase of the axial pressure and the increase of the rotating speed can lead to the increase of the maximum temperature in FSW [13, 14]. The increase of temperature also means the increase of the efficient power in FSW. A nonlinear relation can be found between the increase of the efficient power and the shoulder diameter in FSW [15]. The heat flux in FSW is defined to be functions of rotating speed, axial pressure on the tool and the tool diameters. Hamilton et al. [16] utilize torque based heat input model [17] to develop characteristic temperature curves that correlate temperature data from various aluminum alloys and weld conditions into relationship. A fully coupled thermo-mechanical model is developed [18] to study the temperature rises and the plastic deformations in FSW. A coupled two-dimensional Eulerian thermo-elasto-viscoplastic model is developed [19] for modeling the FSW process. The requirements for torque and power and the geometry of the stirring zone during FSW are modeled by solving the equations of conservation of mass, momentum, and energy [20]. When the heat transfer and the frictional coefficients change, the predicted temperature can still correlate well with the experimental values. For a Norton's friction model developed [21], the great sensitivity of the welding forces and the tool temperatures to the friction coefficients are found. Two contact models are compared and it is found that the modified friction model is more accurate in case of higher angular velocities [22].

Z. Zhang (✉) · J. T. Chen · Z. W. Zhang · H. W. Zhang
State Key Laboratory of Structural Analysis for Industrial Equipment, Department of Engineering Mechanics, Faculty of Vehicle Engineering and Mechanics, Dalian University of Technology, Dalian 116024, China
e-mail: zhangz@dlut.edu.cn

Material flow is also very important in the numerical studies of FSW. It provides a method to investigate the mechanism of FSW. Stream lines, velocity fields, tracer particles are the main methods to reveal the material flows in FSW. The material flows in different depths are different [7]. Using a semi-coupled thermo-mechanical model, Zhang et al. [23, 24] obtained the material flow patterns that can be correlated well with the experimental observations [25–27]. Particles can be traced in the numerical models to directly reveal the material behaviors in FSW [28, 29].

FSW has special advantages in joining thin plates [30–32]. But recent developments of FSW show that FSW can be also applied to joining thick plates in which the thickness of the plates can exceed 6 mm [33–35]. But the differences between FSW of thin plates and of thick plates remain unknown and have not been studied in detail. So, a thermo-mechanical model is used here to investigate the material flows, temperature rises, and energy histories for comparisons of FSW of thin and thick plates.

Model description

In friction stir welding, the welding tool is inserted into the welding plate. After self rotation for several seconds for preheating, the tool starts to move along the welding line with rotations. In current work, 2.5 s is selected for preheating. The material is flowing into the region around the welding tool to simulate the movement of the welding tool in the opposite direction. The movement of the materials of the welding plates for simulation of the movement of the welding tool in opposite direction has been used [28].

The geometrical sizes of the welding tool and the settings of the welding parameters are shown in Table 1. The welding tool is considered to be a rigid body and the density is 7800 kg/m^3. The weld base metal is AA2024-T3. The yield stress is the function of temperature, as shown in Table 2. The density of AA2024-T3 is 2770 kg/m^3. The

Table 1 Geometrical sizes and welding parameters

No.	1	2
Thickness (mm)	3	6.4
Shoulder diameter (mm)	16	20
Pin diameter (mm)	6	7
Axial pressure (MPa)	130	130
Transverse speed (mm/s)	2	2
Rotating speed (rpm)	300	300
Preheating time (s)	2.5	2.5
Weld length (mm)	24	24

Table 2 Yield stress of AA2024-T3

T (°C)	24	100	149	204	260	316	371
σ_s (MPa)	345	331	310	138	62	41	28

heat capacity is 875 J/kg K and the heat conductivity is 120 W/m K. The melting point of AA2024-T3 is 493 °C. According to previous work [29], the frictional coefficient is taken as 0.3 and 90% frictional energy is assumed to enter into the welding plates. Plates with two thicknesses (3 and 6.4 mm) are selected for comparison.

The finite element model of the 3 mm thickness welding plate consists of 9,491 nodes and 8,118 elements. The model of 6.4 mm thickness welding plate consists of 11,281 nodes and 9,881 elements. The meshes and boundary conditions of the finite element model are shown in Fig. 1.

According to energy balance, external work can be converted to kinematic energy, internal energy and frictional energy in FSW,

$$E_W = E_K + E_U + E_F \tag{1}$$

$$E_F = \int_0^t \iint_S p_t \cdot \dot{\gamma} \, dS \, dt \tag{2}$$

$$E_K = \iiint_V \frac{1}{2} \rho \mathbf{v} \cdot \mathbf{v} \, dV \tag{3}$$

The dissipated portions of internal energy E_U are split off into the energy by dissipated viscous effect E_V and the remaining energy E_I,

$$E_V = \int_0^t \left(\int_V \sigma_v : \dot{\varepsilon} \, dV \right) d\tau \tag{4}$$

$$E_I = \int_0^t \left(\int_V \sigma_c : \dot{\varepsilon} \, dV \right) d\tau \tag{5}$$

where σ_c is the stress without viscous dissipation effect. σ_v is the viscous stress. The internal energy includes the elastic strain energy, the energy dissipated by plasticity, and the energy dissipated by time-dependent deformation,

$$E_I = \int_0^t \left(\int_V \sigma_c : \dot{\varepsilon}^e \, dV \right) d\tau + \int_0^t \left(\int_V \sigma_c : \dot{\varepsilon}^p \, dV \right) d\tau$$
$$+ \int_0^t \left(\int_V \sigma_c : \dot{\varepsilon}^c \, dV \right) d\tau \tag{6}$$

where ε^e is the elastic strain, ε^p plastic strain, and ε^c the creep strain.

Fig. 1 Meshes and boundary conditions of finite element model
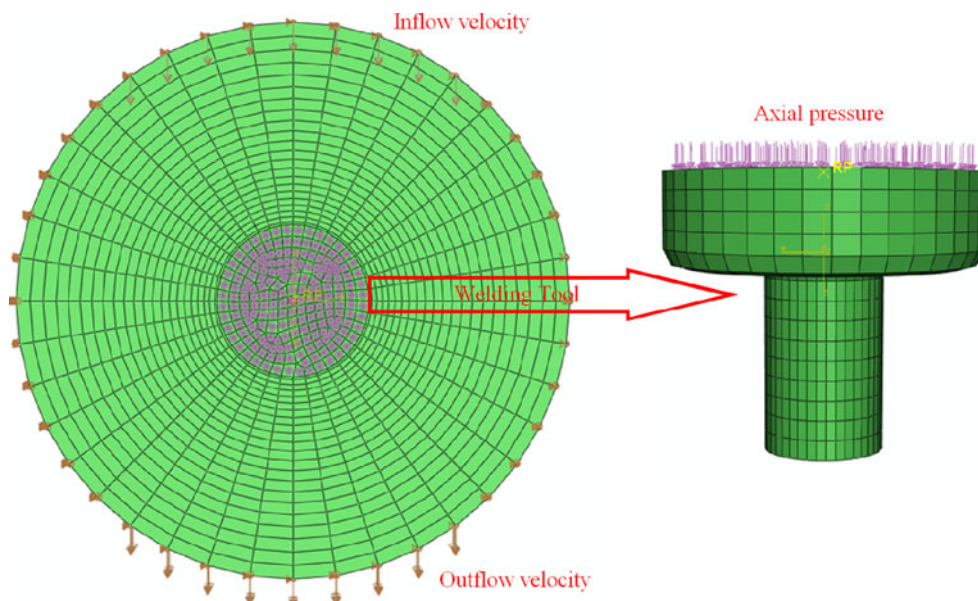
The main contribution to the heat generations in FSW is obviously coming from the friction on the contact surfaces. The friction force can be determined by the multiplication of friction coefficient and contact pressure or the yield stress in current status,

$$\tau_{\mathrm{crit}} = \min(\mu P, \sigma_{\mathrm{s}}/\sqrt{3}) \tag{7}$$

The yield function of the weld base metal AA2024-T3 is,

$$f = \bar{\sigma} - \sigma_{\mathrm{s}}(T) \tag{8}$$

where $\bar{\sigma}$ is the equivalent stress and σ_{s} the yield stress which is the function of temperature shown in Table 1.

The flow rule can be written as,

$$\mathrm{d}\varepsilon^{\mathrm{pl}} = \sum \mathrm{d}\kappa_{\mathrm{i}} \frac{\partial g_{\mathrm{i}}}{\partial \boldsymbol{\sigma}} \tag{9}$$

where $g_{\mathrm{i}}(\sigma, \theta, H_{\mathrm{i},\alpha})$ is the temperature dependent flow potential and $\mathrm{d}\kappa_{\mathrm{i}}$ is a scalar measuring the amount of the plastic flow rate. Predictor–corrector algorithm is used for the solution of strain and stress [28].

According to the Fourier's equation, the temperature can be calculated,

$$\rho c \frac{\mathrm{d}T}{\mathrm{d}t} = \frac{\partial}{\partial x}\left(\lambda_x \frac{\partial T}{\partial x}\right) + \frac{\partial}{\partial y}\left(\lambda_y \frac{\partial T}{\partial y}\right) + \frac{\partial}{\partial z}\left(\lambda_z \frac{\partial T}{\partial z}\right) + q \tag{10}$$

where ρ is the density, c heat capacity, λ the conductivity, and q the heat flux density generated by friction between the welding tool and workpiece,

$$q = p_{\mathrm{t}} \cdot \dot{\gamma} \tag{11}$$

where p_{t} is the frictional stress on the contact surfaces and $\dot{\gamma}$ is the slipping rate. The slipping rate can be determined by

the velocity differences between welding tool and workpiece according to [16, 36],

$$\dot{\gamma} = \delta(r\omega - v_0 \sin\theta) \tag{12}$$

where δ is the slipping factor, ω the rotating speed of the tool, and v_0 the transverse speed of the tool. Compared to the velocity in the tangential direction, the transverse speed is very small. So, the above equation can be simplified as,

$$\dot{\gamma} = \delta r\omega \tag{13}$$

With consideration of the classical Coulomb friction law [22], the heat flux density can be changed to the following form [17, 37],

$$q = \delta\mu P\omega r \tag{14}$$

If heat generation from plasticity is considered, part internal energy can be converted to heat,

$$q_{\mathrm{plastic}} = \eta\sigma_{\mathrm{c}}\dot{\varepsilon}^{\mathrm{p}} \tag{15}$$

where η is the mechanical efficiency which represents the amount of mechanical energy converted to heat. In current work, it is assumed to be 90%.

To avoid mesh distortions, Arbitrary Lagrangian-Euleraian (ALE) method is used. The maps between different configurations play a key role in the ALE finite element formulations [38]. Detailed information on the ALE formulations can be found in [39]. A general finite element package ABAQUS and programs compiled in FORTRAN for the description of the contact model are used for the implementation of the above mentioned model.
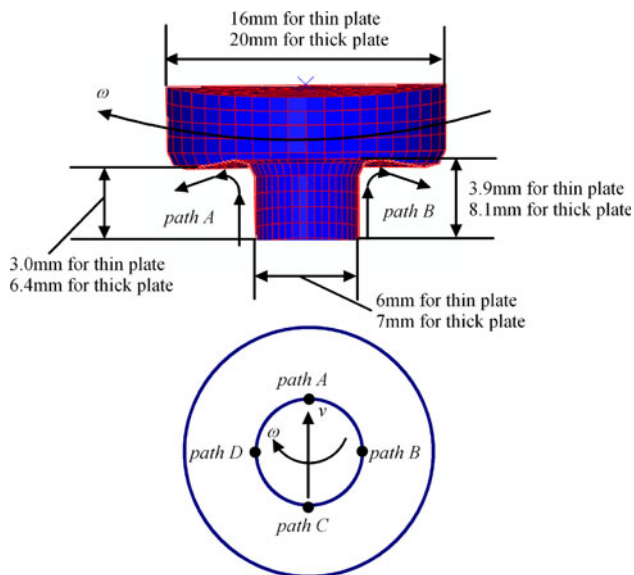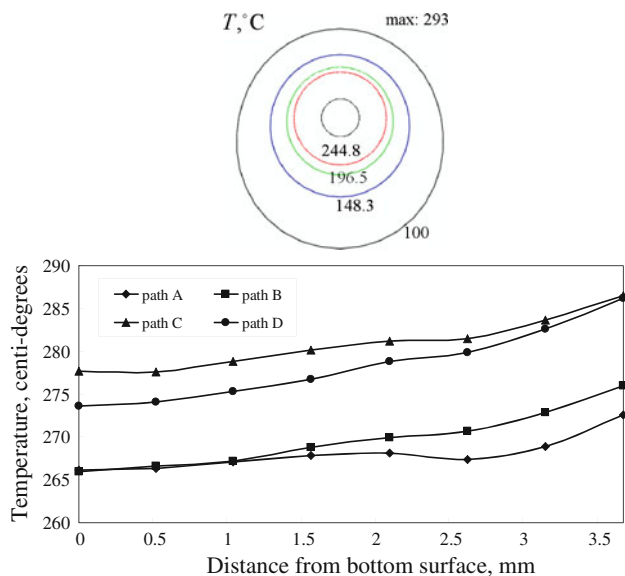
Fig. 2 Selected paths

Fig. 3 Temperature distributions for thin plates

Results and discussions

Four paths are selected for comparisons of material behaviors and temperature variations in different depths of the welding plates, as shown in Fig. 2. Path A is on the front side, path B on retreating side, path C on the trailing side, and path D on the advancing side.

Figure 3 shows the temperature distributions near the welding tool for case 1 listed in Table 1. The maximum temperature is 293 °C and occurs on the shoulder-plate contact surface. From the comparison of the temperatures in different depths, it can be seen that the temperatures on

the trailing and the advancing sides are higher than the ones on the front and the retreating sides. The maximum temperature variation on the top surface is about 10–15 °C. The temperature variation from the top to the bottom surfaces in this case is smaller than 10 °C. The temperature distribution is directly determined by the frictional heat. The frictional heat source can be obtained from the slipping rate and the frictional force. With consideration of material shear failure, the frictional force can be limited by the yield stress [22]. Slipping rate can be calculated from the velocity differences between the welding tool and the welding plates. Based on this point, it can be concluded that the material velocity on the welding plates are not uniform on the contact surfaces. Then, the heat flux into the welding plate is also not uniform on the contact surfaces.

The velocity distribution is shown in Fig. 4. The material flows on the retreating and the front sides are higher. According to Eq. 12, the slipping rate is determined by the velocity differences between welding tool and the workpiece. So, the slipping rates on the retreating and the front sides are lower than the ones on the trailing and the advancing sides. This is the reason that the heat fluxes on the trailing and the advancing sides are higher, which leads to the fact that the temperatures are higher in this region. The maximum velocity is 86.16 mm/s and occurs at intersection of pin-plate and shoulder-plate surfaces on the front side. The velocity is about 50–86 mm/s on the top surface but only 12–18 mm/s on the bottom surface.

Equivalent plastic strain (Fig. 5) is a time-accumulated value. It is not only dependent on the material velocity but also on the time when the material particles are rotated
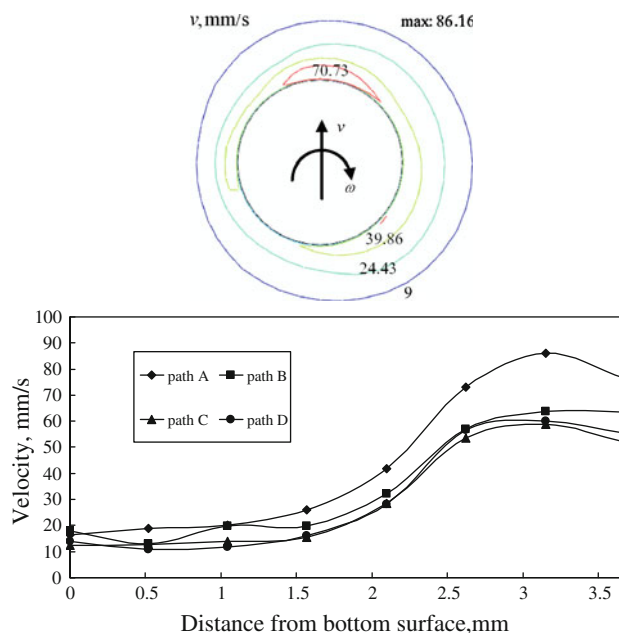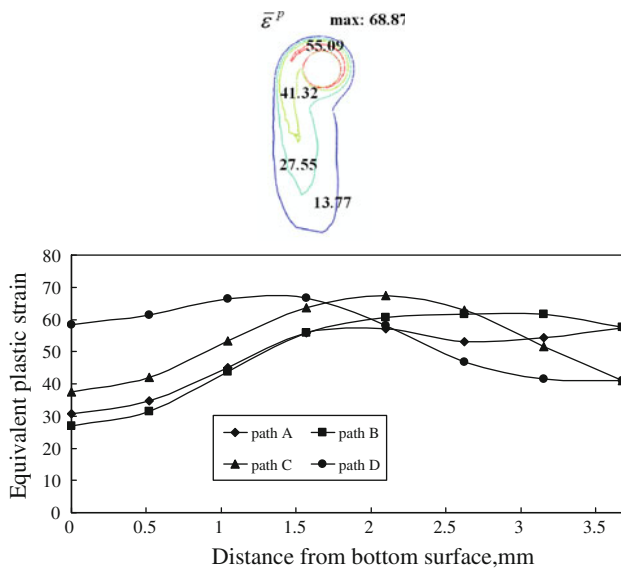

Fig. 4 Velocity field for thin plates

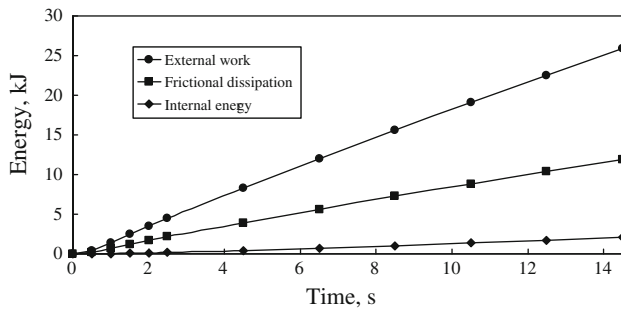Fig. 5 Equivalent plastic strain for thin plates

Fig. 6 Energies for thin plates

Fig. 7 Temperature field for thick plates

around the welding tool. As reported [29], the material on the advancing side can be rotated with the welding pin. After several revolutions, the material particles on the advancing side start to slough off in the wake. From the material flow patterns, it can be concluded that the equivalent plastic strain on the advancing side is higher than the one on the retreating side, which can be validated by the comparison of the equivalent plastic strain between path B and path D. Moreover, the maximum equivalent plastic strain occurs in the middle of the welding plate.

In paths C and D, the plastic deformation and the slipping rate are higher to lead to higher heat flux in this region. So, the temperatures in paths C and D are higher, as shown in Fig. 3.

As studied [34], energies are very important for the fatigue life of the FS welds. So, energy histories should be studied. The energy histories for case 1 are shown in Fig. 6. The energies have quasi-linear relationship with time. So, the efficient power needed for the completion of FSW is
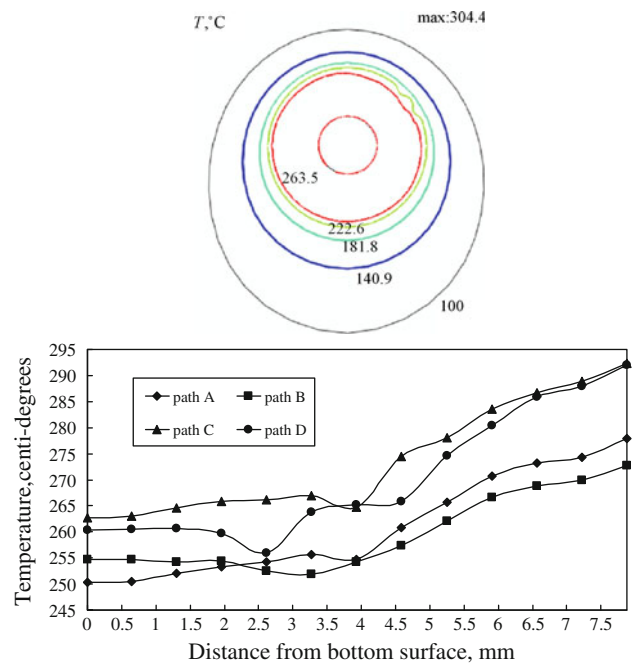
constant. The efficient power is 1.78 kW, the frictional power is 0.82 kW, and the power for the internal energy is 0.14 kW according to Fig. 6. This means that 54% total input energy is transferred to the welding plates and 85.3% can be converted to frictional heat. Both the frictional heat and the plastic deformation can affect the microstructural evolutions in FSW. Based on this point, it can be recognized that the energy efficiency is about 54% in this case.

When the plate thickness is increased to 6.4 mm in case 2, the welding parameters are accordingly adjusted for the success of FSW. The maximum temperature is increased to 304.4 °C, as shown in Fig. 7. Compared to case 1, the temperature difference between the top and the bottom surfaces is apparently increased to about 25–30 °C.

The velocities on the front side and the retreating side are higher than the ones on the advancing side and the trailing side, as shown in Fig. 8. This leads to the fact that the slipping rates are higher on the advancing side and the trailing side. The differences on slipping rates can affect the heat fluxes. So, the temperatures are higher on the advancing side and the trailing side. This is consistent to the observations from Fig. 7. Compared to the case with 3 mm thickness, the maximum velocity is increased from 86.16 to 105 mm/s.

Figure 9 shows the equivalent plastic strain for the thick friction stir weld. The maximum equivalent plastic strain occurs in the middle of the welding plate on the advancing side around the tool. In the wake, the larger values can be transferred to the places near the welding line. The changes are caused by the material flow patterns. The material
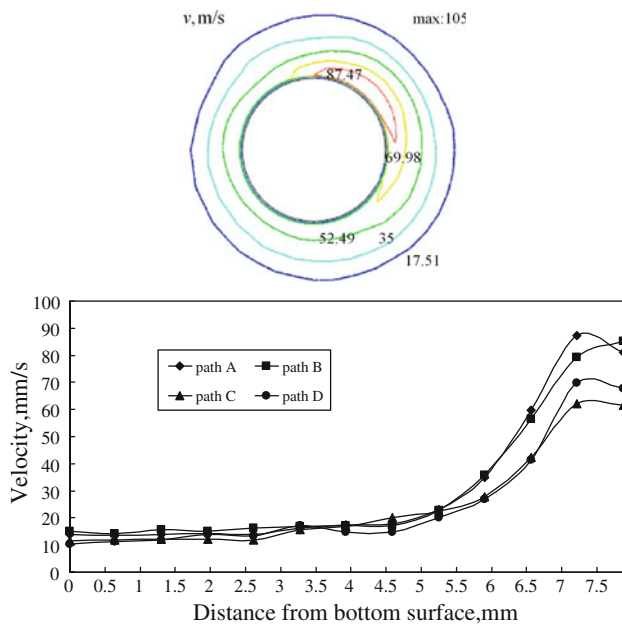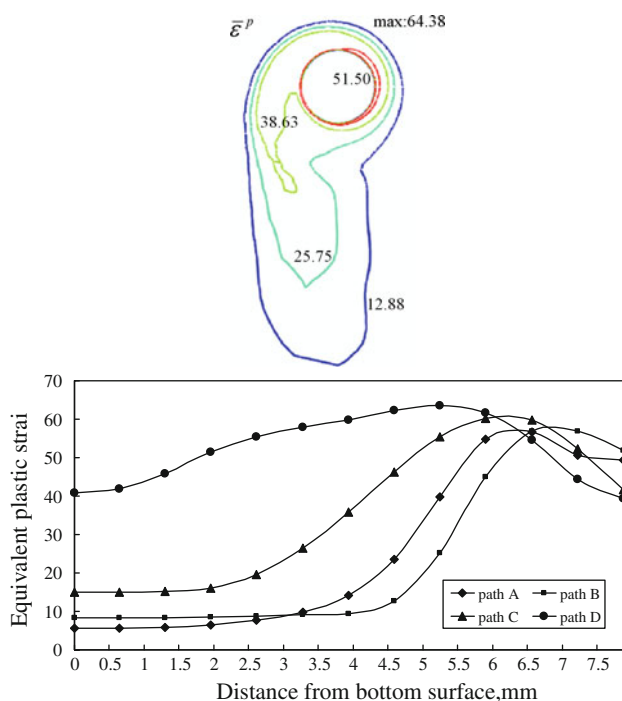
Fig. 8 Velocity field for thick plates

Fig. 9 Equivalent plastic strain for thick plates

particles deposit in the wake on the advancing side near the welding line [29]. Compared to the case for the thin plate, the maximum equivalent plastic strain is decreased to 64.38 although the velocity is higher in this case. The equivalent plastic strain is a time-accumulated value as mentioned above. So, the magnitude of ε^p is not only dependent on the maximum velocity but also the time for
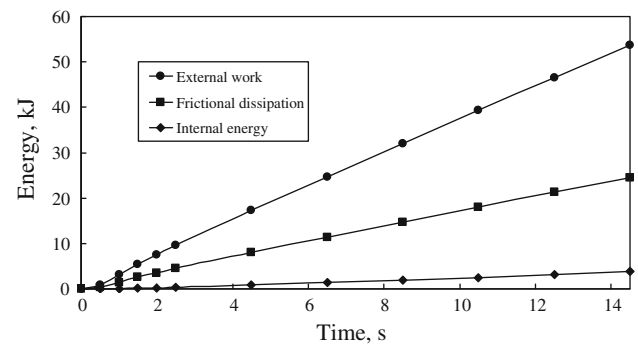

Fig. 10 Energies for thick plates

Table 3 Summarization of computational results

No.	1	2
T_{max} (°C)	293	304.4
$\bar{\varepsilon}^p_{max}$	68.87	64.38
v_{max} (mm/s)	86.16	105
$\dot{E}_W$ (kW)	1.78	3.71
$\dot{E}_F$ (kW)	0.82	1.69
$\dot{E}_F/\dot{E}_W \times 100\%$	46.1%	45.6%
$\dot{E}_I$ (kW)	0.14	0.26
$\dot{E}_I/\dot{E}_W \times 100\%$	7.9%	7%
$(\dot{E}_I + \dot{E}_F)/\dot{E}_W \times 100\%$	54%	52.6%

the material rotations around the welding tool. The decease of the equivalent plastic strain means that the stirring effect of the welding tool becomes weaker in FSW of thick plates. FSW shows advantages in friction stir welding of thin plates based on this point.

The energy histories for FSW of thick plates are shown in Fig. 10. For FSW of thick plates, higher power is needed. The efficient power is increased to 3.71 kW. 45.6% of total energy is converted to frictional heat and 7% is converted to internal energy. Compared to the case of thin plates, the energy entering the welding plate is decreased from 54 to 52.6%.

From the discussions on material deformations and energy histories, it can be seen that the stirring effect becomes weaker and the energy efficiency is decreased in FSW of thick plates. So, based on this point, FSW of thin plates is advantageous. The computational results for both thin and thick plates are summarized in Table 3.

Conclusions

(1) The material flows on the retreating and the front sides are higher. So, the slipping rates on the

retreating and the front sides are lower than the ones on the trailing and the advancing sides. This is the reason that the heat fluxes on the trailing and advancing sides are higher, which leads to that the temperatures are higher in this region.

(2) The maximum equivalent plastic strain occurs in the middle of the welding plate for FSW of AA2024-T3.

(3) More than 50% total energy can be transferred to welding plates and about 85% energy can be converted to frictional heat in FSW of AA2024-T3.

(4) Compared to the case for FSW of thin plate, the maximum equivalent plastic strain is decreased although the velocity is higher in FSW of thick plate. The decease of the equivalent plastic strain means that the stirring effect of the welding tool becomes weaker in FSW of thick plates.

(5) FSW shows advantages in friction stir welding of thin plates with consideration of the material deformations and the energy histories.

References

1. Bhadeshia HKDH, DebRoy T (2009) Sci Technol Weld Join 14:193
2. Cavaliere P, Squillace A, Panella F (2008) J Mater Process Technol 200:364
3. Lorrain O, Serri J, Favier V, Zahrouni H, Hadrouz ME (2009) J Mech Mater Struct 4:351
4. Ma ZY (2008) Metall Mater Trans A 39:642
5. Mahmoud ERI, Takahashi M, Shibayanagi T, Ikeuchi K (2009) Sci Technol Weld Join 14:413
6. Mishra RS, Ma ZY (2005) Mater Sci Eng R 50:1
7. Nandan R, DebRoy T, Bhadeshia HKDH (2008) Prog Mater Sci 53:980
8. Zhou L, Liu HJ (2010) Int J Hydro Energy 35:8733
9. Buffa G, Fratini L, Shivpuri R (2007) J Mater Process Technol 191:356
10. Genevois C, Fabr'egue D, Deschamps A, Poole WJ (2006) Mater Sci Eng A 441:39
11. Simar A, Bre′chet Y, de Meester B, Denquin A, Pardoen T (2007) Acta Mater 55:6133
12. Zhang Z, Zhang HW (2009) Mater Des 30:900
13. Zhang Z, Zhang HW (2009) J Mater Process Technol 209:241
14. Zhang Z, Zhang HW (2007) Sci Technol Weld Join 12:226
15. Zhang Z, Liu YL, Chen JT (2009) Int J Adv Manuf Technol 45:889
16. Hamilton C, Dymek S, Sommers A (2008) Int J Mach Tools Manuf 48:1120
17. Khandkar MZH, Khan JA, Reynolds AP (2003) Sci Technol Weld Join 8:165
18. Schmidt H, Hattel J (2005) Model Simul Mater Sci Eng 13:77
19. Qin X, Michaleris P (2009) Sci Technol Weld Join 14:640
20. Arora A, Nandan R, Reynolds AP, DebRoy T (2009) Scr Mater 60:13
21. Assidi M, Fourment L, Guerdoux S, Nelson T (2010) Int J Mach Tools Manuf 50:143
22. Zhang Z (2008) J Mater Sci 43:5867. doi:10.1007/s10853-008-2865-x
23. Zhang Z, Chen JT (2008) J Mater Sci 43:222. doi:10.1007/s10853-007-2129-1
24. Zhang HW, Zhang Z, Chen JT (2007) J Mater Process Technol 183:62
25. Colligan K (1999) Weld J 78:229
26. Guerra M, Schmidt C, McClure JC, Murr LE, Nunes AC (2003) Mater Charact 49:95
27. Li Y, Murr LE, McClure JC (1999) Scr Mater 40:1041
28. Zhang HW, Zhang Z, Chen JT (2005) Sci Eng A 403:340
29. Zhang Z, Zhang HW (2008) Int J Adv Manuf Technol 37:279
30. Cavaliere P, Campanile G, Panella F, Squillace A (2006) J Mater Process Technol 180:263
31. Dixit V, Mishra RS, Lederich RJ, Talwar R (2009) Sci Technol Weld Join 14:346
32. Peel M, Steuwer A, Preuss M, Withers PJ (2003) Acta Mater 51:4791
33. Lombard H, Hattingh DG, Steuwer A, James MN (2009) Mater Sci Eng A 501:119
34. Lombard H, Hattingh DG, Steuwer A, James MN (2008) Eng Fract Mech 75:341
35. Yan JH, Sutton MA, Reynolds AP (2005) Sci Technol Weld Join 10:725
36. Nandan R, Roy GG, Lienert TJ, DebRoy T (2007) Acta Mater 55:883
37. Chen CM, Kovacevic R (2003) Int J Mach Tools Manuf 43:1319
38. Zhang Z, Zhang HW (2007) Sci Technol Weld Join 12:436
39. Belystchko T, Liu WK, Moran B (2000) Nonlinear finite elements for continua and structures. Wiley, New York, p 393